THE JOURNAL OF PHYSICAL CHEMISTRY C

Article

pubs.acs.org/JPCC

Hydration Structure at the α-Al_2O_3 (0001) Surface: Insights from Experimental Atomic Force Spectroscopic Data and Atomistic Molecular Dynamics Simulations

Dimitrios Argyris,[†] Anh Phan,[†] Alberto Striolo,[†,*] and Paul D. Ashby[‡,*]

[†]School of Chemical, Biological, and Materials Engineering, The University of Oklahoma, Norman, Oklahoma 73019, United States

[‡]Molecular Foundry, Lawrence Berkeley National Laboratory, Berkeley, California 94720, United States

ABSTRACT: Atomic force spectroscopic data obtained in water on the (0001) face of fully hydroxylated α-Al_2O_3 substrate using a silicon tip are presented. The data are obtained by implementing the Brownian force profile reconstruction method (BFPR), originally proposed by Ashby and Lieber [*J. Am. Chem. Soc.***2004**, *126*, 16973]. The method allows for an accurate reconstruction of the high stiffness force−distance curve that highlights the hydration structure. The experimental data are interpreted with the aid of massive atomistic molecular dynamics simulations in which one silicon dioxide disc of ∼2 nm diameter represents the silicon atomic force microscopy (AFM) tip. The umbrella sampling method is employed to obtain the water-mediated surface−disc force profile. It is possible to distinguish two hydration layers confined between tip and surface in both simulations and experiment. Small variations of the disc features yield some differences in the simulated force−distance curve, and the small disc size is responsible for weakening the evidence for the second hydration layer. One dense layer of water molecules is in contact with the α-Al_2O_3 (0001) substrate. This hydration layer yields a pronounced repulsive force when the AFM tip penetrates it, suggesting highly structured interfacial water. The second hydration layer yields much less intense repulsive forces. The position of the peaks with respect to the solid substrate is consistent with recent experimental X-ray reflectivity data reported by Catalano [*Geochim. Cosmochim Acta* **2011**, *75*, 2062] and with previous atomistic simulations conducted for a thin film of water supported on sapphire at ambient conditions by Argyris et al. [*J. Phys. Chem. C* **2011**, *115*, 2038].

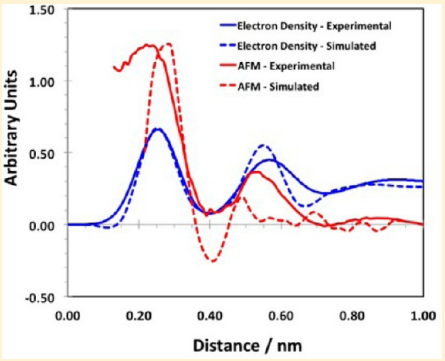

INTRODUCTION

The properties of interfacial water continue to generate enormous interest. Recent reports addressed, among other phenomena, the mechanism by which two hydrophobic surfaces attract each other in water,[1] the effect of atomic-scale roughness and chemical heterogeneity on water sessile contact angle,[2] density fluctuations of water near surfaces,[3] and the relationship between atomic distribution of interfacial water molecules and hydrodynamic slip.[4] Theoretical and experimental approaches are generally attempted in such investigations; each approach has advantages and disadvantages. For example, simulations allow a detailed observation of individual molecules but might suffer from inadequate water−solid force fields and short observation times (simulations longer than ∼100 ns remain prohibitive). Atomic force microscopy (AFM) experiments offer subnanometer spatial resolution but cannot determine absolute tip−surface distances, and it suffers from the probe surface also structuring the solvent and assessing the combined system. X-ray specular reflectivity (XSR) experiments provide molecular-level resolution along the direction perpendicular to the surface but cannot quantify the local orientation of interfacial water molecules. Naturally, each technique is applied to systems that minimize the shortcomings. For example, simulation studies are often conducted on model, sometimes not realistic surfaces,[5,6] and impressive AFM results have been reported for water in contact with mica,[7] a "well-behaved" substrate that is atomically flat and stable.

We investigate here the structure of interfacial water on the (0001) plane of α-Al_2O_3 at ambient conditions [the (0001) plane is also indicated as C-plane, basal plane, and 001 plane in the literature]. We employed a custom-made AFM, using a silicon tip, to sample the structure of interfacial water. We compared the averaged force−distance curves to literature XSR data obtained on the same substrate.[8] We employed massive molecular dynamics (MD) simulations to provide a molecular-level interpretation of the experimental data. Both AFM experiments and MD simulations show force−distance profiles with features that change in response to small differences in either the AFM tip termination or the surface being sampled. The results from the three approaches (AFM, XSR, and MD) are compared, yielding satisfactory agreement. Subtle disagreements on a few details of the observations are important because they suggest hypotheses to be verified in future investigations.

Received: January 11, 2013
Revised: April 22, 2013
Published: April 29, 2013

Our contribution builds on impressive recent developments to understand how the granular structure of water, assessed experimentally already in 1983,[9] determines intermolecular forces.[10−13] Ashby and Lieber[14] proposed the Brownian force profile reconstruction (BFPR) method for extracting the structure of interfacial solvents by accurately recording the probability distribution of tip−surface distances. Alternatively, reconstructing the force profile from frequency and amplitude data in frequency modulation is possible.[15] This method has been used to study the hydration of lipid bilayers,[16] with results qualitatively consistent with molecular simulations.[17] Hiasa et al.[18] investigated water on TiO_2, reporting a number of qualitatively different force−distance curves that suggest the possibility of heterogeneous surface properties. Hiasa et al.[19] studied water on the $(01\bar{1}2)$ plane of α-Al_2O_3. Although they reported a few force−distance curves that differ qualitatively from each other, by combining all curves it is possible to observe several repulsive peaks separated by ∼0.2 nm. This contrasts with experimental data reported for water on mica.[7,20,21] In some cases these results agree remarkably well with atomistic simulations.[22] Another alternative AC technique is amplitude-modulation AFM.[23] This method provides a direct measure of stiffness and damping information, which are related to the effective viscosity of fluid films at an interface.[24]

Interpreting experimental data often requires high-level theoretical approaches.[25] Patrick and Lynden-Bell[26] showed that AFM force−distance profiles can change qualitatively as the tip drifts laterally relative to the surface. Ho et al.[27] suggested that force profiles depend on the properties of the tip apex. Argyris et al.[28] suggested that details of force−distance curves measured on the (0001) α-Al_2O_3 substrate can depend on termination of the solid substrate, formation of hydration layers on both the solid substrate and the AFM tip, and orientation of water molecules within these layers.

The α-Al_2O_3 substrate is chosen for the present work because of its importance for both technological and geochemical applications. Together with iron oxide and other minerals, aluminum oxide is present in soil, sedimentary, and aquatic systems.[29,30] The α-Al_2O_3 (0001) surface is not stable in its O-terminated form. In the presence of water, hydroxyl groups develop, even at low humidity.[31] Sum frequency generation vibrational spectroscopy (SFG) data[32−34] assign the isoelectric point (IEP) near pH 5. SFG data suggest that the surface potential becomes significant for pH < 4 and pH > 7. Second harmonic generation (SHG) data suggest the IEP should be at pH 4.[35] To reconcile these differences, Lutzenkirchen et al.[36] proposed a dual charging mechanism that requires pronounced ordering of interfacial water molecules in contact with the substrate, in agreement with infrared experiments.[37−39]

Structural observations are also important for the present study. Experimental scanning force microscopy shows that the Al_2O_3 surface has a hexagonal structure at high temperature and that the surface is very reactive upon exposure to water vapor.[40] Gan and Franks[41] provided evidence for the presence of edges on the Al_2O_3 surface, reminiscent of hexagonal lattices.

Catalano[8] recently reported specular X-ray reflectivity data for the sapphire−water interface. The results show one dense layer of adsorbed water, with density perturbations that extend for ∼1 nm into the bulk. When compared to the structure of water obtained on (110) and (012) sapphire planes,[42−44] the results suggest that water is less strongly bound on the (001) plane than on the (110) or (012) planes.

Finally, it should be pointed out that Al_2O_3 has been investigated extensively by simulations, mostly using ab initio density functional theory calculations. The results show that the hydroxylated surface is the most stable at ambient conditions in the presence of water.[37,45] Fewer contributions have considered the structure of interfacial water supported on Al_2O_3 via atomistic simulations.[46,47] Not surprisingly, the properties of interfacial water are found to depend on the surface termination.

METHODS

Experimental AFM Force−Distance Curves. In all experiments we used Milli-Q deionized (18.2 MΩ·cm) water for cleaning the surface and for conducting the force spectroscopy measurements. The deionized water has pH ∼7.0. Although the solution pH was not controlled during the experiments, because of the extensive cleaning procedures performed on the surface (described below) and because the AFM experiments were conducted shortly after preparation, it is assumed that the solution pH remained in the range from 7.0 to 5.5, which is comparable to the point of zero charge of the solid sapphire substrate used for the experiments, based on literature reports.[36]

The sapphire (Al_2O_3) C-plane (0001) was used. Single-side-polished single-crystal substrates were purchased from University Wafer (South Boston, MA). The substrates were glued to magnetic AFM pucks with cyanoacrylate glue. The sapphire crystal was first sonicated in acetone (Sigma−Aldrich, ACS reagent-grade, 99.5%) for 20 min and then rinsed with water and dried with nitrogen. Subsequently the surface was placed in a UV/ozone chamber for 30 min, rinsed with water, and dried with nitrogen. The same sonication and UV/ozone steps were repeated by exchanging acetone for ethanol (Sigma−Aldrich, spectrophotomeric grade). The same substrate was used for multiple experiments, and thorough cleaning before each experiment was required to obtain consistent results. All components (AFM tip, tip holder, substrate holder assembly, and tweezers) that came into contact with water during the experiments also required cleaning by rinsing in organic solvent, UV/ozone exposure, rinsing with water, and nitrogen drying.

Force−distance curves were measured with a custom-built low-noise AFM head and an Asylum Research Bipolar controller (Asylum Research, Santa Barbara, CA). The head has very low numerical aperture optics to produce a small spot size on the photodiode (large spot on the cantilever) for high sensitivity.[48] A thermally stabilized superluminescent light-emitting diode (SLED) (Denselight 1270 nm, 20 mW, Singapore) with low 1/f noise was used for deflection detection. The deflection noise measured 2−5 pm rms in a 1 kHz bandwidth and 10 fm/$\sqrt{\text{Hz}}$ noise from 100 to 500 kHz. This enabled the use of relatively stiff cantilevers that had low Q yet were thermal-noise-limited. We used moderate-stiffness silicon AFM probes with resonant frequency ∼30 kHz in water (Budget Sensors, Multi75Al, 3 N/m). The microscope was staged on a vibration isolation table (Table Stable TS-150) and housed in an acoustic isolation enclosure.

Deionized water (∼100 μL) was deposited on the sample, creating a thin water droplet. The AFM tip and tip holder were then brought in close proximity to the surface such that the water droplet wetted the tip holder. The tip holder was not sealed, but no noticeable evaporation took place over the course of each experiment. Amplitude modulation AFM was

used for gentle engagement and imaging, but no cantilever excitation was used during force spectroscopy data collection. Force curves were collected by continuously advancing the sample until a deflection of 1 nm was obtained and then retracting the sample by 10 nm. Velocities of 1 and 2 nm/s were used.

The Brownian force profile reconstruction (BFPR) method[14] enables the reconstruction of accurate force profiles even when the stiffness of the interaction is slightly greater than the stiffness of the cantilever and traditional force curve representations show snap-in. This is because the position distribution of the thermal noise contains information about the energy landscape. For these force spectroscopy experiments we collected the thermal noise by sampling the deflection data at 100 kHz. The reader is directed to ref 14 describing the BFPR method for details, although a short description follows. Each force curve is separated into segments of ∼2K samples which span 3−6 Å of tip−sample distance but only 0.2−0.4 Å of Z piezo displacement. The deflection data are binned into histograms to calculate the probability of each deflection value. Probability is converted to energy via Boltzmann's equation. The energy segments are the sum of the harmonic potential of the cantilever and the tip−sample interaction for multiple steps of the Z piezo. Energy segments far from the surface, where no tip−sample interaction is sampled and only the harmonic potential of the cantilever is present, are fit to determine the cantilever stiffness. The cantilever harmonic potential is then subtracted from all the energy segments to isolate the tip−sample interaction; the derivative is taken to calculate force for each tip−sample distance. These force segments are averaged to create the force profile.

The force−distance curves reported below were obtained by averaging data from ∼45 individual force−distance curves. Approximately 50−80 other curves obtained with the same AFM tip were discarded. In general, the AFM experiments discussed here become less reliable as the experiment continues, because of the accumulation of impurities at the tip and sample. We discarded all force−distance curves that suggest the presence of impurities (large differences between advancing and receding force−distance profiles), all those that show evidence of long-range forces (these should not be present, as we grounded the tip and discharged the surface by blowing ions before assembly), and all those that showed clear evidence of acoustic or mechanical coupling from the environment. Finally, to obtain reliable averages at given substrate−tip distances, the individual force−distance curves were shifted along the distance axis until the second repulsive peaks observed on the various curved overlapped. More details and justifications, including statistical errors, are discussed below. The results presented have been found to be consistent with others obtained with different AFM tips, although the latter were not included in the averaged results shown.

Simulation Models and Algorithms. All simulations presented here were conducted with the simulation package GROMACS, version 4.0,[49,50] in the NVT ensemble (constant number of atoms N, constant volume V, and constant temperature T) following the protocols described previously by Argyris et al.[28,47] Water was simulated by implementing the SPC/E model.[51] The sapphire substrate and the silicon dioxide disc used to mimic the AFM tip were described by use of the CLAYFF force field.[52] Sapphire was considered fully hydroxylated as, during the experiments, the pH of the deionized water should be in the range from 7.0 to 5.5, close to the isoelectric point of the sapphire substrate, so the simulated substrate bears no net charge.

To provide a realistic bridge to the experiments, an AFM tip was modeled as a small disc (∼2 nm in diameter) of amorphous SiO_2. This allowed us to simulate AFM force−distance curves. The SiO_2 disc was prepared following the procedure described by Fan et al.,[53] yielding a surface density of OH groups consistent with that reported for experimental macroscopic amorphous SiO_2 samples. The CLAYFF force field[52] was implemented to describe interactions between the silica disc and the other components in the system. As the point of zero charge for SiO_2 (∼3) is lower than the pH of deionized water used in our experiments, the disc should be negatively charged. To assess how small changes in the AFM termination could affect the measured force−distance curves, we simulated two silica discs. In the first, all the surface OH groups are hydrogenated, yielding a net charge of +4e on the disc. In the second, several surface hydroxyl groups were deprotonated, until the net charge of the SiO_2 disc was 0. When the disc bears a net charge of +4e, four Cl^- ions were added to the simulation box to maintain system electroneutrality.

All simulations were conducted at ambient conditions, mimicking the experimental setup. A thin film of water was deposited on the sapphire substrate, and the SiO_2 disc was immersed in the water film. The simulated system contained 12 000 water molecules. The sapphire substrate was 1.291 nm thick. A total of 49 587 atoms were in the simulation box, including 207 atoms to represent the SiO_2 disc, and 13 376 atoms to represent the solid substrate. To more realistically replicate the experimental force−distance curves, it would be desirable to simulate a larger disc. Such an option, however, would render the simulations intractable with the current computing resources available to us. X and Y dimensions of the simulation box were 9.04 and 9.07 nm, respectively. Equilibrium simulations for water near the sapphire substrate are discussed in details elsewhere.[47]

To construct the potential of mean force between the SiO_2 disc and the alumina surface, we implemented the umbrella sampling algorithm.[54,55] The umbrella sampling procedure is somewhat reminiscent of the Brownian force profile reconstruction (BFPR) method of Ashby and Lieber,[14] used herein to extract force−distance curves from experimental measurements. The algorithm yields the surface−tip potential of mean force as a function of distance. To allow proper comparison with the experiments, the potential of mean force results were differentiated to generate force−distance curves from simulations.

As the disc is assumed to represent an AFM tip, the SiO_2 disc was allowed to vibrate only in the direction perpendicular to the substrate (no rotations were allowed). This causes the resultant force−distance curves to depend on the relative orientation of the disc with respect to the underlying substrate. Also, the center of mass of the disc was forced to remain at given distances from the substrate implementing harmonic springs of various elastic constants. For one SiO_2 disc, 42 independent simulations were conducted, imposing that the equilibrium disc−surface distance changes by 0.05 nm from one simulation to another. At any separation distance the simulation was conducted for up to 8 ns, during which time the histogram representing the distances between the disc center of mass and the substrate was populated. The WHAM algorithm was then used to reconstruct the potential of mean force from combining the histograms obtained at various disc−surface separations.[55]

To satisfy the constraints imposed by the WHAM algorithm, the elastic constants imposed on the center of mass of the disc depended on the distance. At distances of 0.9, 0.95, 1.0, and 1.05 nm between the disc center of mass and the layer formed by the oxygen atoms of the hydroxyl groups on the sapphire surface the elastic constants were 21 000, 39 000, 39 000, and 15 000 kJ/(mol·nm^2), respectively. At larger separations the elastic constant was fixed at 9000 kJ/(mol·nm^2). Higher elastic constants are needed near the surface to allow the silica disc to properly sample the free energy landscape, which is rendered rough by the dense layers of hydration water.

RESULTS

Solid Substrate and AFM Tip Characterization. In the top panel of Figure 1, we show the experimental AFM image of the (0001) α-Al_2O_3 substrate as obtained in water at ambient conditions by AM-AFM imaging. Several steps with rather dendritic edges are present, and some subnanometer depressions are visible throughout the substrate. However, the presence of large terraces with atomically smooth surfaces should allow for the determination of accurate hydration structure.

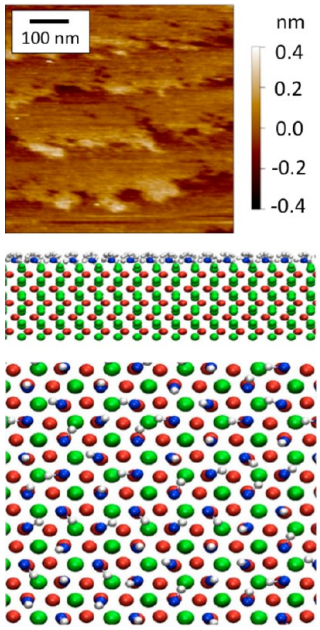

Figure 1. (Top) AFM image of one of the (0001) α-Al_2O_3 samples used for the experimental force−distance curves discussed below. The experiment is conducted with the sample immersed in deionized water at ambient conditions, after careful cleaning procedures have been conducted as described in the Methods section. (Bottom) Schematic of the solid substrate used for the MD simulations; top and side view are both represented. Green and red spheres represent aluminum and oxygen atoms, respectively. Surface hydroxyl groups are highlighted in blue for oxygen and white for hydrogen atoms. Only the upper five atomic layers of the substrate are presented for clarity. X and Y dimensions of the simulation box are 9.04 and 9.07 nm, respectively. Only portions of the simulated substrate are shown. Explicitly, the lateral size of the side view is ∼3.7 nm, while that for the top view is ∼2 nm.

In the bottom panel of Figure 1, we report one schematic representation of the (0001) α-Al_2O_3 substrate used in the atomistic MD simulations. We show top and side views of the alumina substrate, and we highlight the terminal oxygen atoms (blue spheres), which are completely protonated in our simulations, as expected on the basis of ab initio DFT results,[37] yielding hydroxyl groups with a surface density of ∼15 OH groups/nm^2. As discussed previously,[47,56] the distribution and density of the OH groups on the surface determine the structure and mobility of water molecules in contact with the substrate.

When the top and bottom panels of Figure 1 are compared, there is no doubt that the simulated substrate is a simplification of the real system. The AFM image has edges and boundaries that are not accounted for in our simulations. However, the simulated system should be capable of reproducing, at least semiquantitatively, the hydration structure of water near atomically flat and chemically homogeneous surfaces.

In Figure 2, top panel, we show a TEM image of a cantilever employed to conduct the BFPR AFM experiments. The image reveals the crystalline silicon in the core of the tip and the ∼2 nm thick amorphous silicon oxide layer on its surface. The apex radius of curvature is difficult to quantify using only one plane projection but it is estimated to be 2−3 nm. Because the tip is hydrated, some of the oxygen atoms present will be protonated.

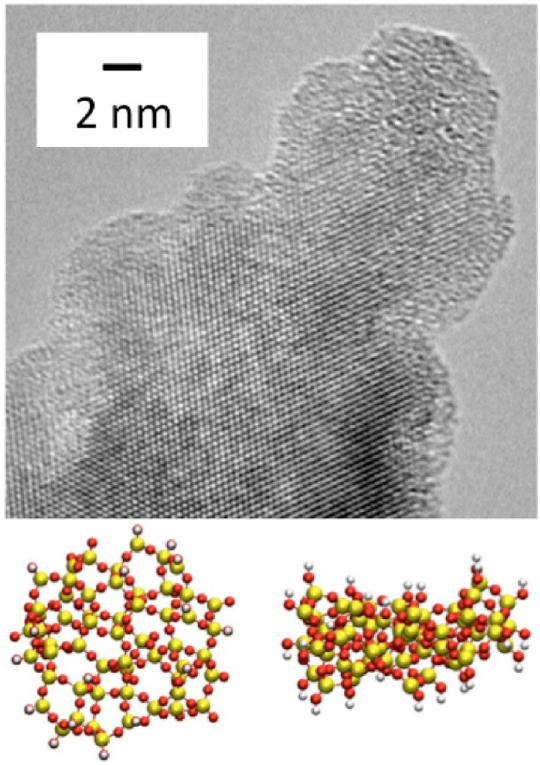

Figure 2. (Top) TEM image of one silicon tip used for the experimental force−distance AFM curves discussed below. The crystalline silicon core is clearly visible, as well as a layer of amorphous silicon oxide ∼2 nm in thickness. (Bottom) Top view (left) and side view (right) of one amorphous SiO_2 disc, fully protonated, used in our simulations to mimic the AFM tip. Yellow, red, and white spheres represent silicon, oxygen, and hydrogen atoms, respectively. The diameter of the simulated silica disc is ∼2 nm.

In the bottom panel of Figure 2, we report a simulation snapshot for one of the amorphous SiO_2 discs that was used to simulate the AFM tip (top and side views are provided). The schematic reproduces Si, O, and H atoms. The thickness of the SiO_2 disc was ∼1.04 nm, and its diameter was ∼2 nm. The SiO_2 disc shown in Figure 2 is the one on which all the nonbridging

dx.doi.org/10.1021/jp400370g | J. Phys. Chem. C 2013, 117, 10433−10444

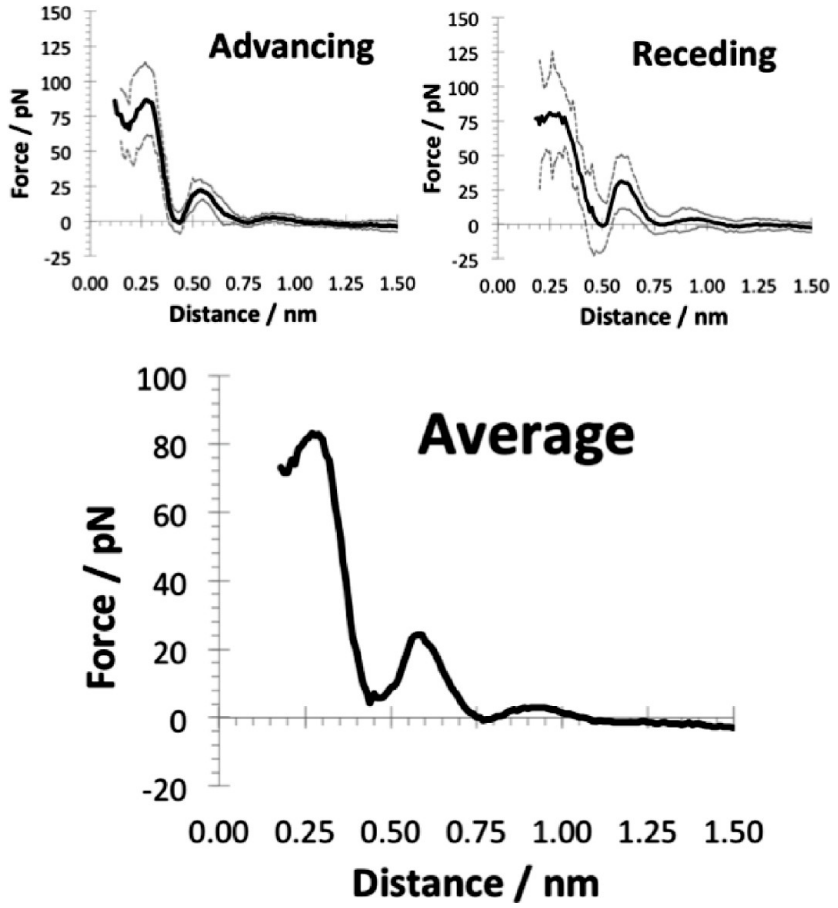

Figure 3. (Top) Experimental BFPR AFM force−distance curves measured in water on the (0001) plane of α-Al_2O_3 substrate. Results in the top left panel are for advancing experiments; the top right panel shows receding experiments. Continuous lines are the averaged results, and dotted lines are obtained by adding and subtracting 1 SD from the averaged results. (Bottom) Experimental BFRP AFM force−distance curves averaged over all available data sets.

O atoms are fully protonated, hence the disc bears a net charge of +4e. The other SiO_2 disc used for our simulations (which does not bear a net charge), not shown for brevity, has a structure comparable to the one shown in Figure 2 except that a few nonbridging oxygen atoms are not protonated.

Although the simulated system does not fully represent the experimental configuration in every detail, the model implemented for the AFM tip is expected to yield insights for the interpretation of experimental force−distance curves. One main difference between real and simulated AFM tip is that, because of computing power limitations, the size of the simulated disc is much smaller than that of the experimental silicon tip. However, we expect a qualitatively valid comparison between simulated and experimental results. The advantage of using a small disc in the simulations is that the size of the simulated system remains tractable (note that 49 587 atoms were simulated). Two possibly more important sources of discrepancies between simulated and experimental results are the surface termination and the net charge imposed on the simulated disc. To assess the magnitude of this possible effect we have considered two different representations of the SiO_2 disc used in the simulations, as discussed in the Methods section. Finally, to better mimic experimental conditions, the SiO_2 disc was not allowed to rotate during the umbrella-sampling simulations and oscillates only along the direction perpendicular to the surface. Thus, the potential of mean force obtained from simulations will depend on the relative orientation between the disc and the surface, as the BFPR experimental results are expected to depend on the relative orientation between the AFM tip and surface.

Experimental AFM Force−Distance Curves. In Figure 3, top left and right panels, we report averaged advancing and receding BFPR force−distance curves obtained from our experiments, respectively. Because of the heterogeneity of the substrate (see Figure 1) and natural drift of the instrument, it is likely that a large number of force−distance curves were collected near step edges and surface defects. Heterogeneities similar to those observed here are likely found on other sapphire substrates, and it is possible that this is responsible for the difficulty in obtaining reproducible force−distance curves, as evidenced by literature reports concerning the α-Al_2O_3 $(01\bar{1}2)$−water interface.[19] We believe that, to quantify the water hydration structure, only experimental data obtained on similar substrates (i.e., atomically flat vs edges) should be used. As discussed in the Methods section, many experimental curves were discarded because they were clearly flawed due to instrument vibration instabilities, trace impurities, drifts, etc. Similarly, the data sets were occasionally truncated before reconstruction to remove anomalous regions, leading to some reconstructions not including transition through the first repulsive peak. To obtain the averaged results shown in Figure 3, the individual curves were shifted along the tip−sample distance axis so that the second repulsive peaks on the various curves overlapped. Unfortunately, the procedure leads to

dx.doi.org/10.1021/jp400370g | J. Phys. Chem. C 2013, 117, 10433−10444

different numbers of individual force measurements at various tip−surface distances. Regarding the curves shown in the top panels of Figure 3, in most cases we collected up to 25 different force measurements for a given distance, but in some cases fewer measurements were available, especially at small tip−surface separations. In such circumstances the experimental uncertainty is rather high. In the top panels of Figure 3, the error is quantified as 1 standard deviation (SD) from the average values when at least five different measurements are available. Since the absolute distance between the tip and the substrate is not measured with AFM, comparison to X-ray reflectivity was used to obtain the approximate absolute distances.

Repulsive forces are associated with the presence of a hydration layer, while attractive forces can in some cases be observed when the tip is in a position that corresponds to the elimination of one hydration layer.[7,20,21,26−28] Because of the large repulsive force, both top panels in Figure 3 suggest the presence of one strongly bound hydration layer in contact with the alumina substrate and a second, less pronounced hydration layer at farther distances. Evidence for a third layer is much weaker. The advancing and receding traces are slightly different, especially for the first hydration layer. For many advancing and receding pairs of force profiles the overlap was good, and for some pairs the overlap was poor. The large force for the first hydration layer suggests that interfacial water molecules are difficult to displace by the AFM tip, and the poor overlap suggests that sometimes when water molecules are displaced they do not easily return to their original positions. The difference between these sets of curves may be due to proximity to steps or defects. The observations summarized in the Introduction suggest that although the Al_2O_3 surface is easily hydroxylated when exposed to water, it may show some degree of morphological heterogeneity (e.g., steps and edges). Because interfacial water strongly responds to heterogeneous surface properties,[57,58] these surface heterogeneities might be responsible for diverse force−distance curves obtained previously by AFM in water.[19] Note that even the force−distance curves obtained for water on mica[7] show differences when data obtained at different lateral positions are compared.

The large variation in our results may be due not only to surface heterogeneity but also to instrument noise and external coupling. By employing more stable instruments and using higher-speed techniques, it might be possible to confirm whether or not the variations of individual measured curves shown in Figure 3 are truly due to heterogeneous surface properties, which would be reflected in a three-dimensional density distribution of water molecules next to the substrate. Such a possibility would be consistent with what has been reported by Fukuma et al.,[7] Loh and Jarvis,[21] and Hiasa et al.,[19] for water on mica. Unfortunately, this is not possible with our results, as lateral tip positions were not recorded during the experiments. Because of the large force distribution associated with our results, we compiled the average force−distance profile obtained from all experiments (bottom of Figure 3). This averaged force−distance curve is used in the remainder of the paper. For clarity, no statistical error is shown on the bottom panel of Figure 3.

To summarize the experimental observations from the bottom panel of Figure 3, the averaged data show a pronounced repulsive peak at distances barely larger than those at which the AFM tip comes in contact with the surface. This first hydration layer is centered at a distance of ∼0.26 nm from the substrate. This peak is tentatively associated with the presence of a tightly bound layer of water molecules in contact with the sapphire surface. The first hydration layer is followed, as the tip−surface distance increases, by a valley in the force−distance curve and then by a second, weaker repulsive peak centered at ∼0.57 nm. This second repulsive peak is tentatively interpreted with the presence of a second hydration layer in the region confined between the AFM tip and the alumina substrate. The fact that the first repulsive peak is significantly more intense than the second is due to the fact that the water molecules sampled in this region are simultaneously in contact with the alumina substrate and the silica AFM tip. They are confined between the surface and the AFM tip and consequently rather difficult to displace. When the distance between surface and AFM tip is such that two water layers can form, water molecules can more easily diffuse, leading to less repulsive forces. This interpretation is consistent with observations on other substrates, summarized in the Introduction.

Simulated Force−Distance Curves. In Figure 4 we report the potential of mean forces (top panel) as obtained from umbrella sampling calculations between two SiO_2 discs (one of which is shown in Figure 2) and the model Al_2O_3 surface of Figure 1. The force between each disc and the surface is numerically calculated by differentiating the potential of mean force results via the three-point differentiation formula.[59] The simulated umbrella-sampling calculations were conducted for the two discs interacting with the alumina substrate while immersed in water. For consistency with data shown in Figure 3, the distance shown in Figure 4 is also obtained by comparison with X-ray reflectivity data. For completeness, we

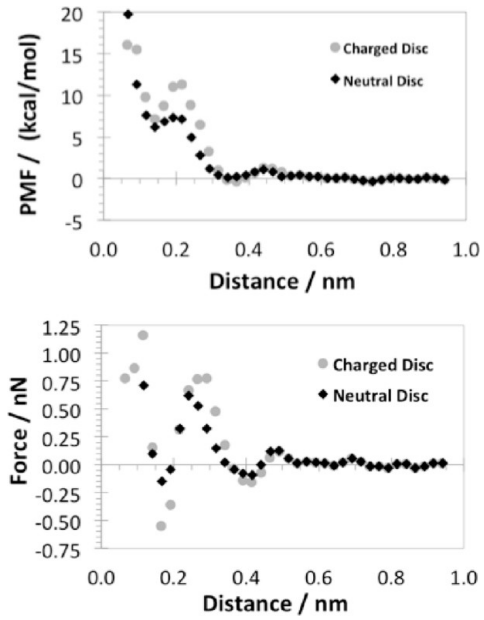

Figure 4. (Top) Simulated potential of mean force as a function of the distance between SiO_2 discs and alumina substrate. Results were obtained by umbrella sampling calculations. (Bottom) Simulated surface−SiO_2 disc force profile obtained by numerically differentiating the potential of mean force data. Black diamonds are for results obtained when the SiO_2 disc is neutral; gray circles are for results obtained when the disc bears a net charge of +4e. Although error bars are not shown for clarity, the oscillations of the force data around the zero baseline at large surface tip−distance in the force−distance curve are representative of the uncertainty in our calculations.

dx.doi.org/10.1021/jp400370g | J. Phys. Chem. C 2013, 117, 10433−10444

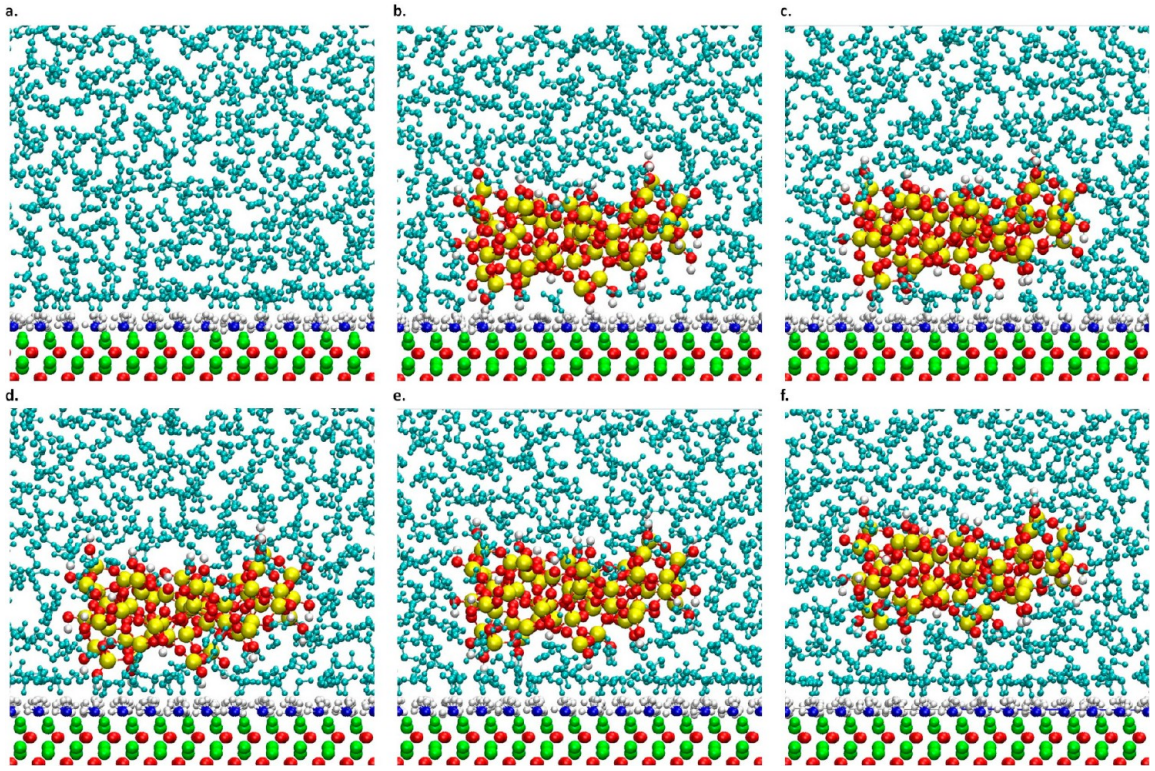

Figure 5. Side views of the silica disc at various distances from the alumina substrate. The disc bears a net charge of +4e. In panel a, the disc is not present. In the other panels, the distance between the disc and the alumina substrate is (b) 0.065, (c) 0.115, (d) 0.165, (e) 0.290, and (f) 0.490 nm. The color schemes for the alumina substrate and the silica disc are the same as those used in Figures 1 and 2. Water is represented as cyan spheres. Only water molecules in the plane identified by the silica disc are shown (those in front of and behind the silica are removed for clarity).

note that the distance between the oxygen atoms of the SiO_2 discs closer to the substrate and the plane formed by the oxygen atoms of the hydroxyl groups in the alumina substrate corresponds to the distance in Figure 4 minus 0.14 nm. The center of mass of the discs is located ∼0.43 nm further from the surface than the distance reported in Figure 4.

The differences between the two sets of data shown in Figure 4 are due to the difference in charge between the two silica discs. In both cases, the force is strongly repulsive at distances below ∼0.14 nm. In the case of the charged disc (gray symbols), the force profile suggests a repulsive plateau at ∼0.1 nm (the force becomes more repulsive at shorter distances, not shown for brevity), while in the case of the neutral disc, the force becomes more and more repulsive as the distance decreases. Visualization of simulation snapshots, discussed below, allows us to conclude that the repulsive forces observed for both discs at such short distances are due to steric repulsions between some of the atoms in the discs and the solid substrate. These interactions were sampled by our experimental AFM probe, but the results, showing many subangstrom steps, were considered too noisy to be included in this paper.

Both data sets in Figure 4 show that the simulated force becomes negative at ∼0.16 nm. The force is significantly more attractive for the charged disc than for the neutral disc.

The disc−surface force becomes repulsive as the distance increases further. In the case of the neutral disc, the repulsive force peaks at distances of ∼0.26 nm and then decreases. For the charged disc, the repulsive force peaks at ∼0.29 nm. For both discs the force becomes slightly negative at distances between 0.34 and 0.44 nm. Then another, much weaker repulsive peak is observed, followed by noise around zero, most likely due to uncertainties in the calculation of the potential of mean force rather than to true physical phenomena.

Comparison of the two force−distance curves shows that both data sets are consistent with a strong repulsive force near the surface (not shown in our experimental data), followed by an attractive region, a second well-pronounced repulsive peak, and a third less pronounced repulsive peak (which, as discussed below, are due to hydration layers). The distance between repulsive peaks attributed to hydration layers in experiments (i.e., the distance between the first and second peaks in Figure 3) is ∼0.3 nm. The analogous distance in simulations (i.e., that between second and third peaks in Figure 4) is ∼0.25 nm. Thus the simulation results systematically show smaller distances between repulsive peaks than their experimental counterparts.

At distances between the first and second hydration peaks (∼0.4 nm in Figure 4), the simulated force−distance profile suggests a relatively strong attraction. This is not evident in the experimental average of Figure 3 at distances ∼0.45 nm but is evident in many of the individual experimental curves (as evidenced by the results shown in the top right panel of Figure 3). It is possible that these discrepancies are due to surface roughness of the material used for our experiments (both alumina surface and AFM tip), compared to the regularity of the substrates used in the simulations, as well as to the rather small size of the simulated SiO_2 disc compared to the experimental AFM tip. However, the qualitative similarity between experimental and simulated force−distance curves allows us to use insights from simulations to interpret some of the features observed in the experiments.

We also note that our simulations show that small variations in the chemical properties of the SiO_2 disc yield significant

dx.doi.org/10.1021/jp400370g | J. Phys. Chem. C 2013, 117, 10433−10444

differences in the details of the force−distance curves. For brevity, we only compare the charged SiO_2 disc data set with the experimental results. The simulated forces are much stronger than the experimental ones. Because experimental data are known to be very sensitive to the tip shape, and because of possible uncertainties due to imperfect force fields and system size effects, we concentrate on force−distance peak shapes and peak positions when we compare data obtained via different tools.

We take advantage of direct observation of representative simulation snapshots to visualize the molecular phenomena responsible for features of the force−distance curve (in simulations, and by extension in experiments). We consider only the system in which the SiO_2 disc bears a net charge of +4e. As will become evident shortly, the simulation results are strongly dependent on the disc features, explaining, in part, the variability in the experimental force−distance curves.

In Figure 5 we present side views of simulation snapshots obtained at various distances between the disc and the α-Al_2O_3 (0001) surface. For comparison, in panel (a) we provide a simulation snapshot in which the disc is not present. The surface−disc distances considered in the other panels are 0.065 nm (panel b), 0.115 (panel c), 0.165 (panel d), 0.290 nm (panel e), and 0.490 nm (panel f). The distance is measured with the same convention as in Figure 4. We focus on the structure of water between the SiO_2 disc and the substrate. When the distance is 0.490 nm (panel f), the simulation snapshot shows that the first layer of water molecules adsorbed onto the alumina substrate is complete and not perturbed by the presence of the SiO_2 disc (compare panel f to panel a). Because the SiO_2 disc has an amorphous contour, it yields only a small enhancement of the water density at the silica surface. These results are not quantified here for brevity, but are consistent with previously reported simulations for water near an amorphous silica sphere.[53] At this distance the SiO_2 disc perturbs the structure of water molecules in the second layer from the alumina substrate. In particular, some of the hydroxyl groups protruding from the disc begin to penetrate the second water layer. The effect is very localized because there are only a few OH groups that extend from the silica disc. However, this perturbation is responsible for the weak peak in the repulsive force observed in Figure 4, at a distance of 0.490 nm. This interpretation is consistent with other simulations.[28]

When the disc−surface distance is 0.290 nm (panel e), some of the OH groups protruding from the disc begin to interact closely with some of the water molecules belonging to the first layer of water adsorbed on the alumina substrate, while other OH groups belonging to the disc have replaced many water molecules in the second hydration layer. Note that in Figure 5 hydrogen and oxygen atoms are shown as having the same size, but in the model the distance between hydrogen and oxygen atoms in the water molecules and surface OH group is 0.1 nm, while the Lennard-Jones diameter of the oxygen atom is 0.3166 nm. The overlap of the hydration layer on the disc with the first hydration layer on alumina yields the strong repulsion predicted by simulations at 0.290 nm (see Figure 4). Similar effects were observed in our prior simulations with a carbon nanotube as the AFM tip.[28]

As the disc−surface distance decreases to 0.165 nm, our simulations predict a rather strong attraction between the disc and alumina substrate (see Figure 4). The simulation snapshot shown in Figure 5d suggests that at this separation the OH groups protruding from the silica disc have substituted some of the water molecules within the first hydration layer on the alumina substrate. These OH groups interact directly with the alumina, possibly forming hydrogen bonds with the surface groups. In addition, the water molecules in the first hydration layer appear not to be perturbed by the presence of the disc. This combination of effects (direct interaction between the silica disc and the surface, and relatively little perturbation of the interfacial water) is likely to yield the strong attractive force predicted by our simulations. Note that results at this and shorter tip−surface distances (discussed in the next paragraph) are not reported in our experimental data.

As the distance is further decreased to 0.115 nm (Figure 5c), one of the OH groups from the silica disc (on the left of the disc) pushes against the layer of hydroxyl groups on the alumina substrate, while some of the other hydroxyl groups are inserted within the first hydration layer. In addition, only a few water molecules are observed in the region between disc and substrate. It is likely that the steric interactions between the OH group of silica and the hydroxyl groups on the surface, combined with the constrained water molecules between disc and substrate, yield the rather strong repulsive force observed in Figure 4 at the distance of 0.115 nm.

As the disc−surface distance decreases further to 0.065 nm, the force−distance curve of Figure 4 shows a slightly less intense repulsion between disc and substrate compared to the results obtained at 0.115 nm. The simulation snapshot of Figure 5B clearly shows that the OH groups of the disc are contacting the substrate, while most of the water molecules have been expelled from the region in between disc and substrate. For complete displacement of the water molecules in the hydration layer, literature predictions and our prior simulation results[28] suggest that an effectively attractive disc−surface interaction should be observed. The data in Figures 4 and 5 suggest that this expected attraction is compensated by a strong steric repulsion due to OH groups of the disc in contact with the substrate. As the distance decreases below 0.04 nm, the disc−surface interaction becomes more repulsive (results not shown for brevity) because the steric effects become dominant. The force fields implemented in the present simulations only allow rotation of the hydrogen atoms in the hydroxyl groups, and therefore as the distance between the disc and the surface is further reduced, the hydroxyl groups on the disc experience strong repulsions due to contact with the solid surface.

The results discussed in conjunction with Figure 5 qualitatively suggest that force−distance curves should depend on the structure of water on the substrate and also on the silica disc; quantitative differences are expected in force−distance curves when different SiO_2 discs are considered, in agreement with data shown in Figure 4. Even more drastic differences are expected when the termination of the disc used for our simulations yields atomically flat versus rough surfaces, as well as when the disc size is increased to replicate experimental AFM tips. As tip orientation with respect to the substrate will affect its termination, the possibility just proposed increases our understanding of why the experimental data suffer from significant variations; i.e., the experimental results are likely to depend on the lateral position of the AFM tip, which changes due to drift.

DISCUSSION: RECONCILIATION BETWEEN DIFFERENT DATA SETS

The absolute distance between tip and surface can be determined with atomistic precision in the simulations, but

the distance in experimental AFM curves is only relative. To satisfactorily compare the experimental to the simulated force profiles, we take advantage of X-ray specular reflectivity data recently reported.[8] In Figure 6 we superimpose the averaged

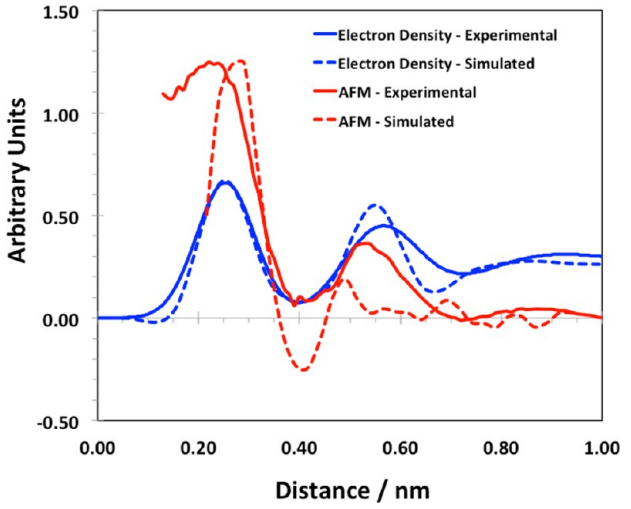

Figure 6. Comparison of experimental and simulation results for structure of hydration water on the (0001) plane of α-Al_2O_3 substrate. (Solid red line) Experimental AFM data obtained in the present work. (Dashed red line) Simulated force−distance profile obtained for the SiO_2 disc that bears a net charge of +4e. (Solid blue line) X-ray reflectivity data reported by Catalano.[8] (Dashed blue line) Electron density for interfacial water as obtained by atomistic simulations on a free-standing, fully hydroxylated crystalline Al_2O_3 substrate.[47] Data in the *Y* axis are scaled to ease comparison, hence they are expressed in "arbitrary units". Based on MD simulation[47] and X-ray reflectivity[8] data, the distance in the *X*-axis is measured from the layer formed by the nonbridging oxygen atoms on the sapphire substrate.

force−distance curve obtained from our AFM experiments (Figure 3), the density profile obtained via X-ray specular reflectivity experiments from Catalano,[8] the simulated force profile of Figure 4, and the simulated electron density extracted from the density profile of oxygen atoms of water as a function of distance from a free-standing completely hydroxylated (0001) alumina surface at ambient conditions we reported recently.[47,56]

Interpreting the X-ray specular reflectivity data, Catalano[8] reported that the layer formed by oxygen atoms of the hydroxyl groups on (0001) α-Al_2O_3 substrate and the layer formed by oxygen atoms of water molecules in the first hydration layer formed on the same substrate are found at 0.0044 and 0.254 nm, respectively, from that of the oxygen atoms belonging to the top layer on the unrelaxed (bulk) substrate. Hence the distance between the first hydration layer and the plane formed by the oxygen atoms of the surface hydroxyl groups in sapphire is ∼0.25 nm. Molecular dynamics simulations show that these two planes are at a distance of 0.26 nm,[47] in good agreement with XSR data. Thus the position of the first peak in the density profile obtained from the X-ray reflectivity data matches the position of the first peak in the density profile of the oxygen atoms of interfacial water molecules obtained from simulations, and both peaks are found at ∼0.25 nm from the plane formed by the oxygen atoms of the hydroxyl groups in the sapphire substrate.

In Figure 6 we superimpose our experimental BFPR AFM data for the hydration structure on the electron density profiles just summarized, as well as the simulated force−distance curve. The force−distance curves, both experimental and simulated, are shifted along the *X* axis so that the first minimum in the force−distance profiles corresponds to the minima in the electron density profiles. For consistency, we adopted this protocol when discussing distances throughout the paper (i.e., Figures 3, 4, and 5). This superposition is chosen because the simulation results of Figure 5 suggests that the first repulsive peak sampled both by experiments and simulations is due to the SiO_2 disc attempting to displace the water molecules in contact with the surface. Both experimental and simulated AFM data show a peak, although the peak is narrower in simulations. When the approaching tip squeezes the hydration layer in between tip and substrate, a repulsive force is expected in AFM experiments.[28] To reconcile the differences between experimental and simulated data, we point out the relatively large experimental uncertainty related to data at close tip−surface distance, which renders it difficult to precisely locate the first peak position.

When the distance is increased slightly, the experimental AFM data suggest that the force in between the first and second repulsive peaks approaches zero and might become attractive. Although many of the curves showed attraction in this region (see top right panel in Figure 3), these were offset by curves that had shallow force wells between the two hydration layers. The simulation snapshots of Figure 5 show that the attraction is due to the fact that the tip in this location has displaced the second hydration layer, which is consistent with simulations obtained on different substrates.[28,60] As mentioned above, evidence of this effect in the force−distance curves is expected to depend on the atomic-scale roughness of both tip and substrate, as well as on the size of the AFM tip. It is likely that using a wide atomically rough tip in the experiments would have prevented us from observing this feature. We also recognize the possibility that uncertainties in the force fields implemented (e.g., the OH groups are rather rigid, as only the H atom is allowed to vibrate) might affect the reliability of the predictions.

Comparing the simulated to the experimental electron density, we find excellent agreement in both position and intensity of the first peak. Comparison for the second peak is also satisfactory, but we note that the simulation data yield a narrower peak. Although this is consistent with other comparisons between experimental and simulated electron density profiles, it is possible that the models used to describe water−surface interactions in the simulations are not capable of correctly reproducing the structure of interfacial water. For example, it is possible that the model alumina substrate yields a hydrogen-bond network between water molecules that differs from the experimental one. Such differences could yield different electron densities beyond the first hydration layer. However, the comparison between simulated and experimental electron density profiles is considered satisfactory, given that no parameter was fit to reproduce the experiments. For completeness, we note that when processing our simulation results, the bin size used to obtain the electron density profile was larger than that used previously to obtain the atomic density profiles.[47,56] Explicitly, the bin size used here was comparable to the diameter of one oxygen atom, while in our prior reports we used bins of size ∼0.1 nm. This was done because electrons are distributed on the entire molecule and not concentrated on the center of the oxygen atoms.

dx.doi.org/10.1021/jp400370g | J. Phys. Chem. C 2013, 117, 10433−10444

The agreement between the position of the first two dense layers of oxygen atoms of water in the reflectivity data and the repulsive peaks obtained from our experiments is good but with clear differences. The first difference is that the distance between peaks is shorter in the AFM experiments. Based on our prior simulations,[28] this observation is consistent with the fact that two surfaces approaching during an AFM experiment (substrate and tip) effectively squeeze the interfacial water layers closer to each other, compared to results obtained on a freestanding surface. We note that although peak-to-peak distances in simulations tend to be shorter than in the corresponding experiments, even the simulations suggest that the distance between the repulsive peaks in the force−distance curve is shorter than that between maxima electron density peaks predicted for water on the freestanding surface.

The intensity of the first peak of the AFM force−distance curves is significantly larger than that of the second peak when compared to results obtained from electron density profiles (both experimental and simulated). On the basis of literature observations,[24] we suspect that it is more difficult to displace the last monolayer of water molecules confined between two surfaces than it is to displace water molecules when two water layers are between the approaching surfaces. As a result, the repulsive force associated with the first hydration layer should be larger than that observed for the second hydration layer. In X-ray reflectivity (both experiments and simulations), water molecules are adsorbed on a freestanding surface, hence such confining effects are not present.

As suggested by the analysis of simulation data, the second repulsive peak in the AFM data is due to interactions between the first hydration layer formed on the alumina substrate and the slightly pronounced first hydration layer formed on the silica tip. As a consequence, it is expected that the repulsive force corresponds to the position of the second hydration layer formed on alumina. This is consistent between experimental and simulated AFM data, although the data in Figure 6 clearly show that the repulsive force of the second hydration layer predicted by our simulations is weaker compared to the one obtained by experiment. It is likely that the experiments yield a more intense second repulsive peak because the AFM tip is much larger than the SiO_2 disc used in the simulations. Maybe for the same reason experimental force peaks are wider than simulated ones, as due in part to tip surface roughness, we expect that the relatively wide tip used in the experiments yields somewhat smoother results, compared to simulation.

Finally, both experimental AFM force−distance data and experimental X-ray reflectivity data suggest the presence of a third weak peak in the profiles shown in Figure 6. This peak is barely visible from the simulation results, and it is found at much closer separations from the surface, suggesting either that the simulation models need to be improved to correctly predict the structure of interfacial water at distances larger than 1−2 monolayers from a solid substrate or that much larger discs are necessary to capture this feature.

SUMMARY AND CONCLUSIONS

We presented experimental force−distance curves obtained with an AFM via the Brownian force profile reconstruction method to characterize the structure of hydration water on the basal plane of sapphire. To enhance the interpretation of the experimental data, we conducted massive atomistic simulations for a silica disc, mimicking the experimental AFM tip, interacting with an atomically smooth, fully protonated alumina substrate. Experimental and simulated force−distance curves are consistent with the formation of a dense first hydration layer of water at contact with sapphire and that of a second hydration layer, perhaps less well-defined than the first one. The position of the peaks, and the distance between them, is consistent with experimental X-ray reflectivity data recently reported in the literature, as well as with atomistic simulations for a thin film of water supported by sapphire. When experiments and simulations are compared, the results show that the distance between first and second repulsive peaks as measured by AFM is shorter than the distance between maxima in electron density profiles, probably a consequence of confining effects experienced by interfacial water as the AFM tip approaches the substrate. Other differences emerge when data from different sources are compared. The differences between experimental and simulated results suggest that improvements might be needed to accurately describe both the structure of the solid substrates and water−water and water−solid interactions to completely capture the properties of hydration water at contact with solid substrates, although simulating larger AFM tips might improve agreement. Nevertheless, the simulation results allow us to describe the molecular reasons for the features observed in our experimental results. These insights were achieved without fine-tuning the force field parameters.

AUTHOR INFORMATION

Corresponding Author

*E-mail pdashby@lbl.gov(P.D.A.) or astriolo@ou.edu (A.S.).

Notes

The authors declare no competing financial interest.

ACKNOWLEDGMENTS

Financial support was provided to the University of Oklahoma by the U.S. Department of Energy, Office of Basic Energy Sciences, under Contract DE-SC0001902. Generous allocations of computing time were provided by the Oklahoma Supercomputer Center for Education and Research (OSCER) and by the National Energy Research Scientific Computing Center (NERSC). Work at the Molecular Foundry and NERSC are supported by the Office of Science of the U.S. Department of Energy under Contract DE-AC02-05CH11231. We thank Virginia Altoe for the TEM image of the AFM tip in Figure 2. A.S. is grateful to Miquel Salmeron of LBNL, where he spent his sabbatical. We thank Professor J. Catalano of Washington University in St. Louis for sharing his X-ray reflectivity data and for constructive criticism during the preparation of this paper.

REFERENCES

(1) Sharma, S.; Debenedetti, P. G. Evaporation Rate of Water in Hydrophobic Confinement. *Proc. Natl. Acad. Sci. U.S.A.* **2012**, *109*, 4365−4370.

(2) Wang, J. H.; Bratko, D.; Luzar, A. Probing Surface Tension Additivity on Chemically Heterogeneous Surfaces by a Molecular Approach. *Proc. Natl. Acad. Sci. U.S.A.* **2011**, *108*, 6374−6379.

(3) Jamadagni, S. N.; Godawat, R.; Garde, S. How Surface Wettabitity Affects the Binding, Folding, and Dynamics of Hydrophobic Polymers at Interfaces. *Langmuir* **2009**, *25*, 13092−13099.

(4) Ho, T. A.; Papavassiliou, D. V.; Lee, L. L.; Striolo, A. Liquid Water Can Slip on a Hydrophilic Surface. *Proc. Natl. Acad. Sci. U.S.A.* **2011**, *108*, 16170−16175.

(5) Striolo, A. From Interfacial Water to Macroscopic Observables: A Review. *Adsorpt. Sci. Technol.* **2011**, *29*, 211−258.

(6) Argyris, D.; Tummala, N. R.; Striolo, A.; Cole, D. R. Molecular Structure and Dynamics in Thin Water Films at the Silica and Graphite Surfaces. *J. Phys. Chem. C* **2008**, *112*, 13587−13599.
(7) Fukuma, T.; Ueda, Y.; Yoshioka, S.; Asakawa, H. Atomic-Scale Distribution of Water Molecules at the Mica-Water Interface Visualized by Three-Dimensional Scanning Force Microscopy. *Phys. Rev. Lett.* **2010**, *104*, No. 016101.
(8) Catalano, J. G. Weak Interfacial Water Ordering on Isostructural Hematite and Corundum (001) Surfaces. *Geochim. Cosmochim. Acta* **2011**, *75*, 2062−2071.
(9) Israelachvili, J. N.; Pashley, R. M. Molecular Layering of Water at Surfaces and Origin of Repulsive Hydration Forces. *Nature* **1983**, *306*, 249−250.
(10) Cleveland, J. P.; Schaffer, T. E.; Hansma, P. K. Probing Oscillatory Hydration Potentials Using Thermal-Mechanical Noise in an Atomic-Force Microscope. *Phys. Rev. B* **1995**, *52*, R8692−R8695.
(11) O'Shea, S. J. Oscillatory Forces in Liquid Atomic Force Microscopy. *Jpn J. Appl. Phys., Part 1* **2001**, *40*, 4309−4313.
(12) Li, T. D.; Gao, J. P.; Szoszkiewicz, R.; Landman, U.; Riedo, E. Structured and Viscous Water in Subnanometer Gaps. *Phys. Rev. B* **2007**, *75*, No. 115415.
(13) Ohnesorge, F.; Binnig, G. True Atomic-Resolution by Atomic Force Microscopy through Repulsive and Attractive Forces. *Science* **1993**, *260*, 1451−1456.
(14) Ashby, P. D.; Lieber, C. M. Brownian Force Profile Reconstruction of Interfacial 1-Nonanol Solvent Structure. *J. Am. Chem. Soc.* **2004**, *126*, 16973−16980.
(15) Sader, J. E.; Jarvis, S. P. Accurate Formulas for Interaction Force and Energy in Frequency Modulation Force Spectroscopy. *Appl. Phys. Lett.* **2004**, *84*, 1801−1803.
(16) Fukuma, T.; Higgins, M. J.; Jarvis, S. P. Direct Imaging of Individual Intrinsic Hydration Layers on Lipid Bilayers at Angstrom Resolution. *Biophys. J.* **2007**, *92*, 3603−3609.
(17) Berkowitz, M. L.; Bostick, D. L.; Pandit, S. Aqueous Solutions Next to Phospholipid Membrane Surfaces: Insights from Simulations. *Chem. Rev.* **2006**, *106*, 1527−1539.
(18) Hiasa, T.; Kimura, K.; Onishi, H.; Ohta, M.; Watanabe, K.; Kokawa, R.; Oyabu, N.; Kobayashi, K.; Yamada, H. Solution-TiO_2 Interface Probed by Frequency-Modulation Atomic Force Microscopy. *Jpn. J. Appl. Phys.* **2009**, *48*, No. 08JB19(03).
(19) Hiasa, T.; Kimura, K.; Onishi, H.; Ohta, M.; Watanabe, K.; Kokawa, R.; Oyabu, N.; Kobayashi, K.; Yamada, H. Aqueous Solution Structure over α-$Al_2O_3(01\bar{1}2)$ Probed by Frequency-Modulation Atomic Force Microscopy. *J. Phys. Chem. C* **2010**, *114*, 21423−21426.
(20) Kimura, K.; Ido, S.; Oyabu, N.; Kobayashi, K.; Hirata, Y.; Imai, T.; Yamada, H. Visualizing Water Molecule Distribution by Atomic Force Microscopy. *J. Chem. Phys.* **2010**, *132*, No. 194705.
(21) Loh, S. H.; Jarvis, S. P. Visualization of Ion Distribution at the Mica−Electrolyte Interface. *Langmuir* **2010**, *26*, 9176−9178.
(22) Leng, Y. S.; Cummings, P. T. Hydration Structure of Water Confined between Mica Surfaces. *J. Chem. Phys.* **2006**, *124*, No. 074711.
(23) Garcia, R.; Perez, R. Dynamic Atomic Force Microscopy Methods. *Surf. Sci. Rep.* **2002**, *47*, 197−301.
(24) Labuda, A.; Grutter, P. Atomic Force Microscopy in Viscous Ionic Liquids. *Langmuir* **2012**, *28*, 5319−5322.
(25) Girard, C. Theoretical Atomic-Force-Microscopy Study of a Stepped Surface: Nonlocal Effects in the Probe. *Phys. Rev. B* **1991**, *43*, 8822−8828.
(26) Patrick, D. L.; Lynden-Bell, R. M. Atomistic Simulations of Fluid Structure and Solvation Forces in Atomic Force Microscopy. *Surf. Sci.* **1997**, *380*, 224−244.
(27) Ho, R. Y.; Yuan, J. Y.; Shao, Z. F. Hydration Force in the Atomic Force Microscope: A Computational Study. *Biophys. J.* **1998**, *75*, 1076−1083.
(28) Argyris, D.; Ashby, P. D.; Striolo, A. Structure and Orientation of Interfacial Water Determine Atomic Force Microscopy Results: Insights from Molecular Dynamics Simulations. *ACS Nano* **2011**, *5*, 2215−2223.
(29) Brown, G. E.; Henrich, V. E.; Casey, W. H.; Clark, D. L.; Eggleston, C.; Felmy, A.; Goodman, D. W.; Gratzel, M.; Maciel, G.; McCarthy, M. I.; et al. Metal Oxide Surfaces and Their Interactions with Aqueous Solutions and Microbial Organisms. *Chem. Rev.* **1999**, *99*, 77−174.
(30) Cornell, R. M.; Schwertmann, U. *The Iron Oxides: Structure, Properties, Reactions, Occurences, and Uses*: Wiley−VCH: New York, 2003.
(31) Eng, P. J.; Trainor, T. P.; Brown, G. E.; Waychunas, G. A.; Newville, M.; Sutton, S. R.; Rivers, M. L. Structure of the Hydrated α-Al_2O_3 (0001). *Surf. Sci.* **2000**, *288*, 1029−1033.
(32) Braunschweig, B.; Eissner, S.; Daum, W. Molecular Structure of a Mineral/Water Interface: Effects of Surface NanoRoughness of α-Al_2O_3 (0001). *J. Phys. Chem. C* **2008**, *112*, 1751−1754.
(33) Florsheimer, M.; Kruse, K.; Polly, R.; Abdelmonem, A.; Schimmelpfennig, B.; Klenze, R.; Fanghanel, T. Hydration of Mineral Surfaces Probed at the Molecular Level. *Langmuir* **2008**, *24*, 13434−13439.
(34) Zhang, L.; Tian, C.; Waychunas, G. A.; Shen, Y. R. Structures and Charging of α-Alumina (0001)/Water Interfaces Studied by Sum-Frequency Vibrational Spectroscopy. *J. Am. Chem. Soc.* **2008**, *130*, 7686−7694.
(35) Fitts, J. P.; Shang, X. M.; Flynn, G. W.; Heinz, T. F.; Eisenthal, K. B. Electrostatic Surface Charge at Aqueous/α-Al_2O_3 Single-Crystal Interfaces as Probed by Optical Second-Harmonic Generation. *J. Phys. Chem. B* **2005**, *109*, 7981−7986.
(36) Lutzenkirchen, J.; Zimmermann, R.; Preocanin, T.; Filby, A.; Kupcik, T.; Kuttner, D.; Abdelmonem, A.; Schild, D.; Rabung, T.; Plaschke, M.; et al. An Attempt to Explain Bimodal Behaviour of the Sapphire C-plane Electrolyte Interface. *Adv. Colloid. Interfac. Sci.* **2010**, *157*, 61−74.
(37) Thomas, A. C.; Richardson, H. H. Growth of Thin Film Water on α-Al_2O_3 (0001): An FTIR Study. *J. Phys. Chem. C* **2008**, *112*, 20033−20037.
(38) Thomas, A. C.; Richardson, H. H. 2D-IR Correlation Analysis of Thin Film Water Adsorbed on α-Al_2O_3 (0001). *J. Mol. Struct.* **2006**, *799*, 158−162.
(39) Al-Abadleh, H. A.; Grassian, V. H. FT-IR Study of Water Adsorption on Aluminum Oxide Surfaces. *Langmuir* **2003**, *19*, 341−347.
(40) Barth, C.; Reichling, M. Imaging the Atomic Arrangements on the High-Temperature Reconstructed α-Al_2O_3 (0001) Surface. *Nature* **2001**, *414*, 54−57.
(41) Gan, Y.; Franks, G. V. High Resolution AFM Images of the Single-Crystal α-Al_2O_3 (0001) Surface in Water. *J. Phys. Chem. B* **2005**, *109*, 12474−12479.
(42) Catalano, J. G.; Park, C.; Zhang, Z.; Fenter, P. Termination and Water Adsorption at the α-Al_2O_3 (012)−Aqueous Solution Interface. *Langmuir* **2006**, *22*, 4668−4673.
(43) Catalano, J. G.; Fenter, P.; Park, C. Interfacial Water Structure on the (012) Surface of Hematite: Ordering and Reactivity in Comparison with Corundum. *Geochim. Cosmochim. Acta* **2007**, *71*, 5313−5324.
(44) Catalano, J. G. Relaxations and Interfacial Water Ordering at the Corundum (110) Surface. *J. Phys. Chem. C* **2010**, *114*, 6624−6630.
(45) Lodziana, Z.; Norskov, J. K.; Stoltze, P. The Stability of the Hydroxylated (0001) Surface of α-Al_2O_3. *J. Chem. Phys.* **2003**, *118*, 11179−11188.
(46) Li, C. L.; Choi, P. Molecular Dynamics Study of the Adsorption Behavior of Normal Alkanes on a Relaxed α-Al_2O_3 (0001) Surface. *J. Phys. Chem. C* **2007**, *111*, 1747−1753.
(47) Argyris, D.; Ho, T. A.; Cole, D. R.; Striolo, A. Molecular Dynamics Studies of Interfacial Water at the Alumina Surface. *J. Phys. Chem. C* **2011**, *115*, 2038−2046.
(48) Ashby, P. D. Direct Mapping of Intermolecular Interaction Potentials. In *Handbook of Molecular Force Spectroscopy*; Noy, A., Ed.; Springer: New York, 2008; pp 273−285.

(49) Hess, B.; Kutzner, C.; van der Spoel, D.; Lindahl, E. GROMACS 4: Algorithms for Highly Efficient, Load-Balanced, and Scalable Molecular Simulation. *J. Chem. Theory. Comput.* **2008**, *4*, 435−447.
(50) Van der Spoel, D.; Lindahl, E.; Hess, B.; Groenhof, G.; Mark, A. E.; Berendsen, H. J. C. GROMACS: Fast, Flexible, and Free. *J. Comput. Chem.* **2005**, *26*, 1701−1718.
(51) Berendsen, H. J. C.; Grigera, J. R.; Straatsma, T. P. The Missing Term in Effective Pair Potentials. *J. Phys. Chem.* **1987**, *91*, 6269−6271.
(52) Cygan, R. T.; Liang, J. J.; Kalinichev, A. G. Molecular Models of Hydroxide, Oxyhydroxide, and Clay Phases and the Development of a General Force Field. *J. Phys. Chem. B* **2004**, *108*, 1255−1266.
(53) Fan, H.; Resasco, D. E.; Striolo, A. Amphiphilic Silica Nanoparticles at the Decane−Water Interface: Insights from Atomistic Simulations. *Langmuir* **2011**, *27*, 5264−5274.
(54) Torrie, G. M.; Valleau, J. P. Monte-Carlo Free-Energy Estimates Using Non-Boltzmann Sampling: Application to Subcritical Lennard-Jones Fluid. *Chem. Phys. Lett.* **1974**, *28*, 578−581.
(55) Kumar, S.; Bouzida, D.; Swendsen, R. H.; Kollman, P. A.; Rosenberg, J. M. The Weighted Histogram Analysis Method for Free-Energy Calculations on Biomolecules. 1. The Method. *J. Comput. Chem.* **1992**, *13*, 1011−1021.
(56) Phan, A.; Ho, T. A.; Cole, D. R.; Striolo, A. Molecular Structure and Dynamics in Thin Water Films at Metal Oxide Surfaces: Magnesium, Aluminum, and Silicon Oxide Surfaces. *J. Phys. Chem. C* **2012**, *116*, 15962−15973.
(57) Argyris, D.; Cole, D. R.; Striolo, A. Hydration Structure on Crystalline Silica Substrates. *Langmuir* **2009**, *25*, 8025−8035.
(58) Giovambattista, N.; Debenedetti, P. G.; Rossky, P. J. Enhanced Surface Hydrophobicity by Coupling of Surface Polarity and Topography. *Proc. Natl. Acad. Sci. U.S.A.* **2009**, *106*, 15181−15185.
(59) Carnahan, B.; Luther, H. A.; Wilkes, J. O. *Applied Numerical Methods*; Wiley: New York, 1969.
(60) Striolo, A.; Chialvo, A. A.; Cummings, P. T.; Gubbins, K. E. Water Adsorption in Carbon-Slit Nanopores. *Langmuir* **2003**, *19*, 8583−8591.